



# Impact of Flow Unsteadiness on Turbine Airfoil Heat Transfer via Streaming

**Tapish Agarwal**

Technion - Israel Institute of Technology,  
Haifa 32000, Israel  
e-mail: tapish@technion.ac.il

**Ian Jacobi**

Technion - Israel Institute of Technology,  
Haifa 32000, Israel  
e-mail: ijacobi@technion.ac.il

**Beni Cukurel<sup>1</sup>**

Technion - Israel Institute of Technology,  
Haifa 32000, Israel  
e-mail: beni@cukurel.org

*Thermal management of turbine airfoils is a critical design consideration, but the impact of unsteadiness on heat transfer of attached flow regions has received less attention in the literature. When turbine surfaces are subjected to unsteady zero-mean flow fluctuations, either naturally or artificially, the mean velocity around them is modified due to a nonlinear interaction of fluctuations, known as streaming. In this numerical study, we examine the effect of streaming on heat transfer and skin friction in a simplified model of the flow over a turbine blade. Both heat transfer and skin friction modifications were found to strongly depend on the amplitude and wave speed of the unsteady flow perturbations. Over a wide range of disturbance parameters, skin friction modification was negligible, but a significant effect on heat transfer due to streaming was identified. Moreover, the impact of favorable pressure gradients, which are typical for turbine airfoils, on the streaming phenomena was also considered, and it was found that flow regions of zero-pressure gradient produced the strongest amplification of heat transfer, although the effect of the pressure gradient varied with Strouhal number. Due to its significant effect on wall heat transfer, the streaming phenomenon should be taken into account during the design and measurement of the thermal properties of unsteady systems. [DOI: 10.1115/1.4065123]*

*Keywords: unsteady flows, boundary layers, steady streaming, heat transfer, Reynolds decomposed simulations, numerical methods, turbine external flows, boundary layer development, fluid dynamics and heat transfer phenomena in compressor and turbine components of gas turbine engines*

## 1 Introduction

Characterizing the effect of flow unsteadiness on heat transfer of turbine blades has significant practical implications for the geometry of blades, material selection, and flow control strategies. But recent reviews of the state of art in computational fluid dynamics (CFD) have indicated that there is significant room for improvement in the predictive capabilities of CFD, even for relatively simple flow scenarios, such as an uncooled airfoil in a cascade configuration [1]. And capturing subtle heat transport effects with large eddy simulation (LES) can be challenging and may require the use of high spatial and temporal discretization, resulting in high computational costs. Therefore, most studies have been experimental. But experiments also pose significant challenges, particularly with respect to identifying the sources of various influences on the heat transfer properties of the flow.

Han et al. [2] conducted an experimental investigation on the influence of unsteady wakes on heat transfer from a gas turbine blade. They found that the heat transfer is strongly dependent

on both the Reynolds number and the Strouhal number of the passing wake, and that it increased with both parameters. In addition, they found that the heat transfer at a fixed Reynolds number was solely a function of the Strouhal number, regardless of the rod speeds or number of blades. Reference [3] noted that in some cases, the presence of unsteady wakes resulted in higher heat transfer despite no apparent change in separation and reattachment behavior. Reference [4] presented a similar observation of an increase in heat transfer coefficient with the increasing Reynolds number. They also found that wake frequency was positively correlated with increased heat transfer at low turbulence intensity, but the results were inconclusive for higher turbulence intensity. In all of these studies, researchers observed that naturally occurring unsteady effects appeared to exert a significant influence on heat transfer, but did not fully explore the phenomenon.

Unsteady effects can also emerge artificially through flow control methods. The flow control techniques often involve the use of periodic flow disturbances, such as synthetic jets, mechanical flaps, or plasma actuators, or more comprehensive techniques such as acoustics [5]. These disturbances are used to trigger or amplify natural instability mechanisms, e.g., Kelvin–Helmholz. Or they can be used to control separating and re-attaching shear layers [6,7], thereby reducing the reattachment length. Although most of these flow control approaches aim to control separating flows, the attached flow can also be modified by modifying the flow near

<sup>1</sup>Corresponding author.

Contributed by the International Gas Turbine Institute (IGTI) of ASME for publication in the JOURNAL OF TURBOMACHINERY. Manuscript received July 10, 2023; final manuscript received March 14, 2024; published online April 4, 2024. Tech. Editor: David G. Bogard.

the wall, where high-temperature gradients can be created without significantly affecting the overall pressure loss. A classical way of modifying the near-wall flow in a boundary layer is through the introduction of periodic perturbations [8].

When zero mean, periodic velocity fluctuations (modes) are introduced to the flow near the wall, they interact nonlinearly via advection with themselves generating (or modifying) a net mean flow, which is referred to as streaming. This streaming effect is highly dependent on the type of modes introduced to the wall region: temporal, traveling, or standing. In particular, travelling-wave modes can behave very differently from standing waves: if a travelling wave convects at a velocity smaller than the freestream flow, then there exists a wall-normal location, where the phase speed of the perturbation matches the local mean velocity, which exhibits a singularity under a linearized, inviscid stability analysis using the Rayleigh equation. The singularity at this critical point is ultimately resolved by the action of viscosity in a thin layer about the singularity, called the critical layer, as described by the viscous Orr–Sommerfeld equation. Generation of this layer substantially amplifies the effect on the near-wall region, as was discussed in Ref. [9]. It was shown that these critical layer effects can result in significant modification of the skin friction over a simple flat plate boundary layer.

Different types of the downstream, travelling-wave disturbances that can result in critical layers can occur naturally in typical turbine systems, as discussed in Sec. 4. In this study, we explore how such natural travelling disturbances in a model turbine blade system can influence the friction/heat transfer behavior, as a function of the phase speed and amplitude of the disturbances, as well as the pressure gradient over the turbine blade. In Sec. 2, we outline the forced, unsteady boundary layer system, and in Sec. 3, we propose a numerical solution, which is an extension of the procedure adopted by Ref. [10]. In Sec. 4, we explore the range of physical parameters for disturbances relevant for turbine blade conditions. Finally, we report the effect of these unsteady disturbances on skin friction in Sec. 5 and heat transfer in Sec. 6, followed by a discussion of important findings in Sec. 7 and a brief conclusion in Sec. 8.

## 2 Governing Equations

A disturbance in the form of a finite-amplitude traveling wave was introduced to a model flow of a turbine blade. von Karman and Millikan first proposed using a flat geometry with a linearly varying freestream velocity as a simple representation for the flow over an airfoil [11]. This flow, often referred to as Howarth flow [12] or a “single-roof” flow, captures the accelerating or decelerating flow associated with the pressure or suction regions of an airfoil, respectively, and allows for matching the freestream velocity at the trailing edge of the body.

Following von Karman and Millikan, the laminar flow was modeled using Prandtl’s boundary layer equation. However, due to the oscillatory motion of the freestream, stricter assumptions about the Reynolds number were needed to ensure that the boundary layer assumption was valid, as discussed in Ref. [13]. The boundary layer equation was then split into mean and fluctuating velocity fields using a Reynolds decomposition. These fields were solved numerically to explore how the traveling wave disturbance affected the mean velocity profile.

The instantaneous velocity field ( $\hat{u}$ ,  $\hat{v}$ ) was nondimensionalized according to  $(u, v) = (\hat{u}, \hat{v})/\hat{U}$ . The coordinates were nondimensionalized as  $(x, y, t) = (\hat{x}/\hat{\ell}, \hat{y}/\hat{\ell}, \hat{t}\hat{\omega})$ , and the pressure was nondimensionalized as  $p = \hat{p}/\hat{\rho}\hat{U}^2$ , where  $\hat{p}$  is the fluid density, assumed constant. The instantaneous temperature field was nondimensionalized to have the same boundary conditions as the streamwise velocity,  $\Theta = (\hat{\Theta} - \hat{\Theta}_w)/(\hat{\Theta}_\infty - \hat{\Theta}_w)$ .

The nondimensional instantaneous momentum equation is rewritten using an inertial stretching,  $(u, v, \Theta, X, Y, T) = (u, v, \Theta, xRe, yRe, tRe/St_c)$ , and capital letters here represent

stretched coordinates. This choice of coordinates results in a perturbation velocity of the form  $u_1 = u_1/[cRe_1]^{-1}(X - cT)$  and a free-stream velocity of

$$u_\infty(X, T) = (1 - a_p X Re_1^{-1}) + \varepsilon u_1/[cRe_1]^{-1}(X - cT) \quad (1)$$

where  $a_p$  is the acceleration parameter representing the presence of a pressure gradient in the domain, and  $\varepsilon$ ,  $Re_1$ , and  $c$  are domain independent and constitute the three fundamental parameters of the system. For  $a_p < 0$ , the flow is accelerating (favorable pressure gradient) and for  $a_p > 0$ , the flow is decelerating (adverse pressure gradient). For modeling purposes, we focus on the favorable pressure gradient regions of the flow, to avoid the complication of separation behavior.

Using the stretched coordinates, a Reynolds decomposition was performed, allowing the mean boundary layer equation to be written as follows:

$$\bar{u} \frac{\partial \bar{u}}{\partial X} + \bar{v} \frac{\partial \bar{u}}{\partial Y} = -\frac{\partial \bar{p}}{\partial X} + \frac{\partial^2 \bar{u}}{\partial Y^2} + \varepsilon^2 \underbrace{\left( -u' \frac{\partial u'}{\partial X} - v' \frac{\partial u'}{\partial Y} \right)}_{f(X, Y)}, \quad (2)$$

$$\bar{v}(X, Y) = -\int_0^Y \frac{\partial}{\partial X} \bar{u}(X, s) ds$$

The fluctuating dynamics can similarly be written as follows:

$$\frac{\partial u'}{\partial T} - \frac{\partial^2 u'}{\partial Y^2} - \frac{\partial u_1}{\partial T} = \left( \frac{\partial u_1}{\partial X} - \bar{u} \frac{\partial u'}{\partial X} - \bar{v} \frac{\partial u'}{\partial Y} \right) + \left( -u' \frac{\partial \bar{u}}{\partial X} - v' \frac{\partial \bar{u}}{\partial Y} \right) + \varepsilon \left\{ \left( u_1 \frac{\partial u_1}{\partial X} - u' \frac{\partial u'}{\partial X} - v' \frac{\partial u'}{\partial Y} \right) - f(X, Y) \right\},$$

$$v'(X, Y) = -\int_0^Y \frac{\partial}{\partial X} u'(X, s) ds \quad (3)$$

For the detailed derivation of these equations, refer to Ref. [9].

Following the same procedure of Reynolds decomposition, the equations governing the temperature dynamics in the domain were derived for the mean flow:

$$\bar{u} \frac{\partial \bar{\Theta}}{\partial X} + \bar{v} \frac{\partial \bar{\Theta}}{\partial Y} = \frac{1}{Pr} \left( \frac{\partial^2 \bar{\Theta}}{\partial Y^2} \right) + \varepsilon^2 \underbrace{\left( -u' \frac{\partial \Theta'}{\partial X} - v' \frac{\partial \Theta'}{\partial Y} \right)}_{f_\Theta(X, Y)} \quad (4)$$

and for the temperature fluctuations:

$$\frac{\partial \Theta'}{\partial T} - \frac{1}{Pr} \left( \frac{\partial^2 \Theta'}{\partial Y^2} \right) = \left( -\bar{u} \frac{\partial \Theta'}{\partial X} - \bar{v} \frac{\partial \Theta'}{\partial Y} \right) + \left( -u' \frac{\partial \bar{\Theta}}{\partial X} - v' \frac{\partial \bar{\Theta}}{\partial Y} \right) + \varepsilon \left\{ \left( -u' \frac{\partial \Theta'}{\partial X} - v' \frac{\partial \Theta'}{\partial Y} \right) - f_\Theta(X, Y) \right\} \quad (5)$$

These equations were solved in a rectangular domain subject to the following boundary conditions:

$$(X, Y = 0): \quad u' = v' = \Theta' = \bar{u} = \bar{v} = \bar{\Theta} = 0$$

$$(X = 0, Y): \quad u' = u_1(-Re_1^{-1}T), \quad v' = \Theta' = 0, \quad \bar{u} = \bar{\Theta} = 1, \quad \bar{v} = 0 \quad (6)$$

$$(X, Y \rightarrow \infty): \quad \bar{u} = (1 - a_p X Re_1^{-1}), \quad \bar{\Theta} = 1$$

Although the choice of a no-slip velocity boundary condition is straightforward, the boundary conditions for the fluctuating temperature at the wall typically require additional consideration. Different groups have considered the question of how to fix wall boundary conditions for heat fluctuations over the years, and the consensus [14,15] is that an isothermal boundary condition is applicable when interested in only the mean quantities without

focusing on the coherent structure of the wall fluctuations. Because in this study, we resolve only the mean heat flux and the averaged fluctuations, there would be no way to extract structural features from wall fluctuations. Therefore, we follow the accepted procedure for mean field calculations where we assume an isothermal wall.

### 3 Numerical Approach

The mean momentum equation, (2), depends on a mean forcing term,  $f(X, Y)$ , which depends on the dynamic fluctuations of momentum. Therefore, the mean momentum equation was solved iteratively through the following steps:

- Initialization: The mean momentum equation was first solved assuming  $f(X, Y) = 0$ , to obtain an initial guess of the mean momentum balance. This initial guess was used to solve the fluctuating dynamics, (3), for  $u'$  and  $v'$ , from which  $f(X, Y)$  was calculated. This forcing term was then substituted back into the mean dynamics, (2), to calculate an initial estimate of the mean momentum balance with all terms accounted for. The newly calculated mean flow variables,  $(\bar{u}, \bar{v})$ , were then used to obtain a corrected estimate of the fluctuating balance with all terms included. This completes the initialization.
- Prediction–correction iteration: The fluctuating dynamics, (3), were iterated in a prediction–correction procedure until a converged solution was found at each time-step.
- Time marching: The fluctuating dynamics were advanced in time, and the prediction–correction iteration was repeated at the new time-step. This process was repeated until a full period of the fundamental frequency was completed.
- Convergence check: The full period calculation itself was then repeated until convergence. Once convergence was achieved,  $f(X, Y)$  was recalculated and the mean momentum balance, (2), was updated. The updated mean momentum equation was then fed into the fluctuating dynamics, and the entire process was repeated until the mean balance converged.

The converged fluctuating and mean velocity components were used as inputs for the mean, (4), and fluctuating, (5), temperature equations. These equations were subsequently solved using the same iterative approach as the momentum equation.

The system of momentum and temperature equations was solved using finite differences on a rectangular domain in the streamwise direction from  $X = 0$  to  $X = 10^6$ . The domain was divided into eight streamwise blocks due to memory constraints, and each block was solved sequentially using the exit conditions of the upstream block as the inlet conditions for the downstream block. The domain in the wall-normal direction extended from  $Y = 0$  to  $Y \approx 10\sqrt{X}$ , which is approximately two times the downstream boundary layer thickness of each block. The mean momentum balance equation was discretized using a second-order, space-centered implicit finite difference scheme in the wall-normal direction and a first-order, backward scheme in the streamwise direction. This implicit finite difference formulation was solved using a fast tri-diagonal matrix algorithm. The mean quantities obtained were used as input for the fluctuating flow equation, which was solved using a time marching method with an iterative prediction–correction approach. The grid resolution and time-steps were chosen to satisfy the grid convergence index method and the Courant–Friedrichs–Lewy number was kept below 0.5 for stability. The calculations were performed using MATLAB on a four-core desktop computer for a duration of about one day per  $X/10^6$ . The mean skin friction coefficient was defined as the derivative of the mean flow velocity near the wall and had a numerical uncertainty of 0.3%.

The use of the Reynolds-decomposed numerical technique on the boundary layer equations allowed for significantly faster calculation times compared to direct numerical solutions of the full momentum equations. The nondimensional parameters

governing the simulations were selected based on the range of values observed in experimental studies of turbine blade performance.

### 4 Relevant Range of Parameters

The nondimensional model flow system depends on the Reynolds' number,  $X$ , Prandtl number,  $Pr$ , streaming Reynolds' number,  $Re_1$ , amplitude of velocity fluctuations,  $\epsilon$ , wave–speed of disturbances,  $c$ , and the pressure gradient/acceleration parameter,  $a_p$ . For turbomachinery applications, in place of the Reynolds number, a more intuitive nondimensional parameter is the Strouhal number, which can be written as a function of streamwise distance,  $St_x = X/Re_1$ . Therefore, the set of independent parameters can be written as  $(Pr, a_p, c^{-1}, St_x, Re_1, \text{ and } \epsilon)$ ; relevant ranges for each parameter follow.

The Prandtl number,  $Pr$ , depends on the temperature of the air in the turbine. A typical axial flow turbo jet engine has a turbine inlet temperature of 1300K [16], which corresponds to  $Pr$  between 0.71 and 0.74.

The acceleration parameter,  $a_p$ , is associated with the pressure gradient on the turbine blade. The suction side of turbine airfoils have been reported to exhibit favorable pressure gradients on the order of  $\partial C_p / (\partial \hat{x} / \hat{C}) \sim -3.4$  in the forward section and adverse pressure gradients on the order of  $\partial C_p / (\partial \hat{x} / \hat{C}) \sim 2$  in the aft section. The pressure side was observed to exhibit a favorable pressure gradient on the order of  $\partial C_p / (\partial \hat{x} / \hat{C}) \sim -2.2$  across the extent of the blade [17]. These pressure gradients correspond to acceleration parameter  $a_p$  in the range of  $-0.05$  to  $+0.02$ .

The convection velocity,  $c^{-1}$  is associated with the movement of coherent momentum or vorticity structures in the flow over the turbine blade. Large-scale coherent structures in the turbine flow field can propagate at various speeds depending on their size and intensity and the background flow field in which they are convecting. For example, Ref. [18] found that stall vortices from NACA airfoils convect at a speed between 30% and 40% of the freestream velocity,  $u_\infty$  (which means  $c^{-1} = 2.5$  to  $3.3$ ) depending on their pitch rate. In an experimental study on propagation of cylinder wakes, Ref. [19] found that the convection speed increases from  $0.53u_\infty$  to  $0.84u_\infty$  ( $c^{-1} = 1.2$  to  $2$ ) as the vortex convects downstream and then saturates. This convection velocity was found to be the same for transitional and turbulent wakes. Very large-scale motions in turbulent boundary layers tend to convect at around  $0.8u_\infty$  very near the wall, where they exert a footprint on the near-wall flow field [20]. All of these considerations result in a range of  $c^{-1}$  between 0 and 3.3.

The Strouhal number,  $St_x$ , and streaming Reynolds number,  $Re_1$ , depend on the frequencies associated with the wake of the turbine blade. The wake of turbine blades at a high subsonic Mach number has been observed to exhibit a frequency of approximately 7.6 kHz with a maximum amplitude of 90% of downstream dynamic pressure [21]. Reference [22] report an oscillation of 6–9% of velocity amplitude in between the second stator and second rotor at the blade passing frequency of 1.8 kHz in a two-stage axial turbine. This translates to a relevant streaming Reynolds number,  $Re_1$  in the range of  $10^4$ – $10^5$ , and a fluctuation amplitude,  $\epsilon$  (relative to the freestream velocity), which can range from 0.06 to 0.1, or even higher in some cases. The magnitude of resulting Strouhal number,  $St_x$  based on distance along a typical blade chord is up to 50.

These characteristic ranges of turbomachinery parameters were used in the numerical simulations of the model flow field, described earlier. A summary of these parameters is provided in Table 1.

### 5 Skin Friction Modification

Travelling-wave disturbances in the freestream generate streaming near the wall of the turbine blade, which modifies the skin friction and heat transfer. These resultant changes are a function of the

**Table 1** Range of nondimensional parameters for the numerical campaign

Variable	Values
Inverse wave speed, $c^{-1}$	-4 to 4
Amplitude of oscillations, $\epsilon$	0.01 to 0.1
Reynolds number, $Re$	up to $10^6$
Streaming Reynolds number, $Re_1$	$10^4$ to $10^5$
Acceleration parameter, $a_p$	-0.05 to 0
Strouhal number, $St_x$	0 to 50

full set of independent parameters ( $\epsilon$ ,  $c^{-1}$ ,  $St_x$ ,  $a_p$ ,  $Pr$ , and  $Re_1$ ), but we first focus on the effect of  $St_x$  and  $c^{-1}$  on the skin friction and then return to the influence of the remaining parameters.

The change in skin friction can be quantified as the relative variation of the skin friction coefficient with respect to the unforced flow case,  $\Delta\bar{C}_f$ , normalized by the skin friction coefficient for the unforced flow,  $\bar{C}_{f0}$ .  $\Delta\bar{C}_f/\bar{C}_{f0}$  as a function of  $c^{-1}$  and  $St_x$  is shown in Fig. 1. A highly nonmonotonic behavior, consisting of islands of significant increases and decreases in relative skin friction, is observed. Let us consider the region of upstream traveling waves,  $c^{-1} < 0$ : a relative decrease in skin friction is observed, the magnitude of which increase with  $St_x$  and the absolute value of  $c^{-1}$ . For a small input disturbance, with amplitude,  $\epsilon$ , equal to 1% of the freestream velocity, as much as a 4% decrease in skin friction is observed. For the region of downstream traveling waves, the variation is similar except for an island of relative increase in skin friction appearing around the intersection of critical and Stokes' layers. The intersection of these two physical layers results in a change in sign of the relative skin friction variation. Again, for an input disturbance with amplitude equal to 1% of the freestream velocity, an increase in skin friction of the order of 4% is observed for this set of conditions. For detailed analysis of this skin friction behavior, including a discussion of how the skin friction modification varies with the input disturbance amplitude, refer to Ref. [9].

As discussed in Sec. 4, several wave speeds are possible for the disturbances in a turbine specific environment, caused by upstream traveling waves, acoustic waves, convecting wakes, or shed vortices, corresponding to typical inverse wave speeds  $c^{-1}$  of -1.3, 1, 1.6, and 2.8, respectively. Constant convection velocity slices of the relative skin friction modification were extracted from Fig. 1 at four selected wave speeds of interest (marked by horizontal lines), and the corresponding profiles are shown in Fig. 2(a). Note that when disturbances are convected at exactly the local mean velocity,  $c^{-1} = 1$ , there is no effect on the skin friction,

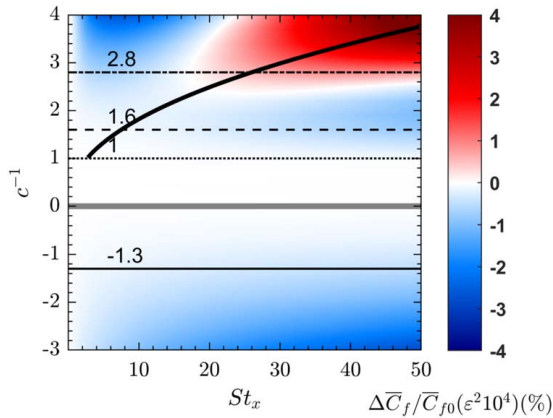


**Fig. 1** Relative change in skin friction  $\Delta\bar{C}_f/\bar{C}_{f0}$ , as a function of inverse wave speed and Strouhal number, for  $(\epsilon, b^*, Pr, Re_1) = (0.01, 0, 0.71, 2 \times 10^4)$ ; horizontal lines show wave speeds of interest for thermal calculations; and the solid curve shows intersection of Stokes' and critical layers

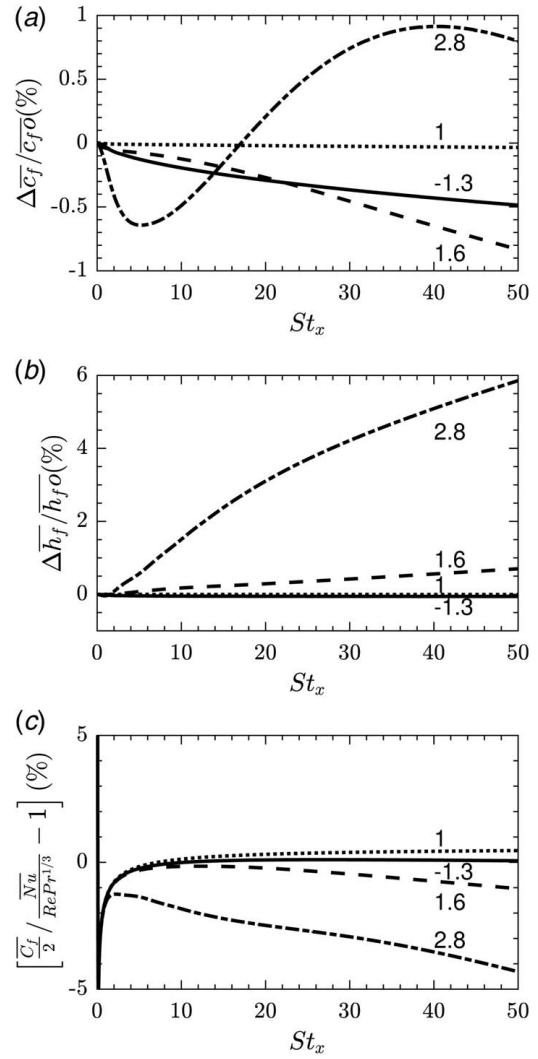


**Fig. 2** (a) Relative change in skin friction coefficient  $\Delta\bar{C}_f/\bar{C}_{f0}$ , (b) relative change in heat transfer coefficient or Nusselt Number  $\Delta\bar{h}_f/\bar{h}_{f0}$ , and (c) deviation from Chilton–Colburn form of the Reynolds' analogy (which corrects for  $Pr \neq 1$ ), as a function of wave speed and Strouhal number, for  $(\epsilon, a_p, Pr, Re_1) = (0.01, 0, 0.71, 2 \times 10^4)$

whereas the downstream travelling wave with  $c^{-1} = 2.8$  exhibits a strong increase in skin friction. The strong increase is associated with the generation of a critical layer, which significantly increases the amplitude of near-wall velocity fluctuations, and ultimately the near-wall mean velocity. On the other hand, upstream traveling wave,  $c^{-1} = -1.3$ , and waves representing wakes,  $c^{-1} = 1.6$ , result in a skin friction decrease of the order of  $-1\%$ .

## 6 Heat Transfer Modification

The numerical approach for the velocity calculations based on Ref. [10] was further extended to the calculations of temperature, by solving the laminar thermal equations as laid out in Sec. 2. To the present authors' best knowledge, only Ref. [13] reported solving these thermal equations for fluctuating quantities and only in the case of temporal wave oscillations. We found that streaming effects for traveling waves are significant, while it was negligible for temporal waves. The temperature equations presented in Sec. 2 subject to isothermal wall boundary condition were solved to find the relative change in the heat transfer coefficient ( $\Delta\bar{h}_f/\bar{h}_{f0}$ ), which is shown for the wave speeds of interest in Fig. 2(b). Heat

transfer modification exhibited a different dependence on  $c^{-1}$  and  $St_x$  compared to skin friction, especially for downstream traveling waves. Unlike the islands of nonmonotonic behavior for the skin friction,  $\Delta\bar{h}_f/\bar{h}_{f0}$  varied monotonically with  $St_x$  and  $c^{-1}$ . For downstream traveling waves with amplitude only 1% of the freestream velocity, the heat flux from the surface increased by as much as 6%, nearly an order of magnitude stronger than the relative effect on skin friction, whereas the heat flux decreased by up to 0.3% for upstream traveling waves. This indicates that significant modification of heat transfer is associated with downstream traveling waves of high  $c^{-1}$  and at large  $St_x$ .

Because the variation in heat flux does not parallel the skin friction modification as a function of  $St_x$  and  $c^{-1}$ , the Reynolds analogy tends to break down when subjected to these travelling disturbances, as illustrated in Fig. 2(c). This divergence can be attributed to fact that the velocity disturbances interact nonlinearly with themselves (Eq. (2)), whereas the temperature fluctuations simply amplify the effect of the velocity fluctuations (Eq. (4)), without any nonlinear damping. It was also observed that changes in skin friction as well as heat transfer are not a function of the streaming Reynolds number  $Re_1$ . The reason for this independence can be ascribed to the fact that frequency dependence is already built into the  $St_x$  parameter; therefore, there is no separate scaling with  $Re_1$ .

**6.1 Effect of Amplitude.** As noted earlier, both skin friction and heat transfer enhancements depend on the imposed amplitude of fluctuations. The analysis above considered only small, 1% amplitude disturbances and still observed significant changes to the heat flux, by as much as 6%. Figure 3(a) shows how the relative change in heat transfer coefficients scales for different amplitudes of oscillations, indicating the much larger variations in heat flux can result from even modestly larger amplitude perturbations. Figure 3(b) shows that these heat flux profiles collapse for different perturbation amplitudes,  $\epsilon$ , when scaled with  $\epsilon^2$ , thus illustrating

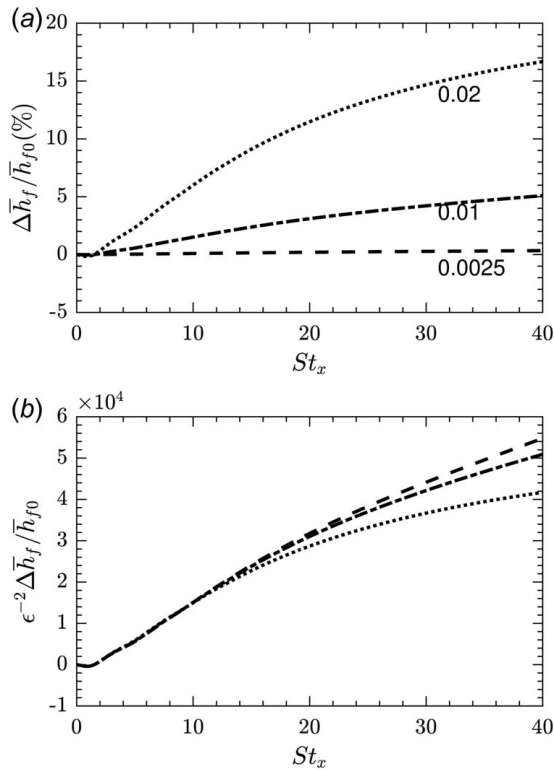


**Fig. 3** (a) Relative change in heat transfer coefficient  $\Delta\bar{h}_f/\bar{h}_{f0}$ , as a function of  $St_x$  for three values of fluctuation amplitude  $\epsilon$  and (b) relative thermal enhancement divided by  $\epsilon^2$ , for  $(c^{-1}, a_p, Pr, Re_1) = (2.8, 0, 0.71, 2 \times 10^4)$ , respectively

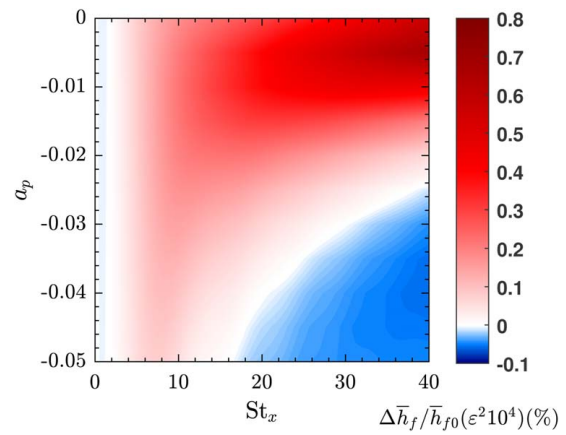


**Fig. 4** Relative change in heat transfer coefficient  $\Delta\bar{h}_f/\bar{h}_{f0}$ , as a function of acceleration parameter  $a_p$  and  $St_x$ , for  $(\epsilon, c^{-1}, Pr, Re_1) = (0.01, 1.6, 0.71, 2 \times 10^4)$ , respectively

how small increases in the amplitude can result in quadratically larger changes in the heat flux modification.

**6.2 Effect of Favorable Pressure Gradient.** In turbomachinery applications, the flow over a blade usually experiences a favorable pressure gradient on the pressure side. On the suction side, the front part of the blade experiences a favorable pressure gradient and the aft part experiences an adverse pressure gradient. In addition, the pressure gradient at the leading and trailing stagnation points is zero. Therefore, as a function of the pressure gradient, a turbine blade can be divided into five zones: pressure side, front suction side, aft suction side, leading edge, and the trailing edge. Here, we present the effect of the favorable and zero-pressure gradients on the heat flux modification via streaming.

The varying favorable pressure gradients over the range of values relevant for turbomachinery applications are represented by the acceleration parameter,  $a_p < 0$ . Figure 4 shows the relative change in heat flux as a function of  $a_p$  and  $St_x$  for a disturbance convection velocity of  $c^{-1} = 1.6$ . Figure 5 shows the same map for a disturbance convection velocity of  $c^{-1} = 2.8$ . In both cases, the forcing amplitude is limited to 1% of the freestream velocity. These nondimensional results can be physically interpreted for a developing boundary layer with a freestream flow velocity of 100 m/s, with coherent fluctuations of 1 m/s at 4.4 kHz, resulting in an increase in the heat transfer coefficient of 5% for zero-pressure gradient

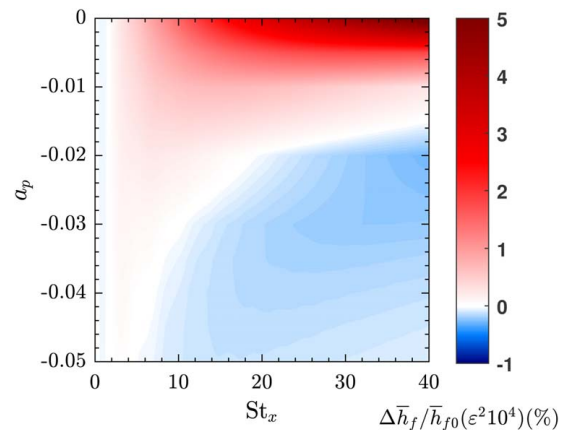


**Fig. 5** Relative change in heat transfer coefficient  $\Delta\bar{h}_f/\bar{h}_{f0}$ , as a function of acceleration parameter  $a_p$  and  $St_x$ , for  $(\epsilon, c^{-1}, Pr, Re_1) = (0.01, 2.8, 0.71, 2 \times 10^4)$ , respectively

conditions, decreasing to only a 0.5% increase for a favorable pressure gradient of  $6 \times 10^3$  Pa/m.

As observed earlier, the lower speed downstream disturbances, associated with slow-moving, large-scale coherent flow features, exert the strongest overall impact on the heat transfer. And the maximum modification of the heat transfer occurs in the region of a zero-pressure gradient and decreases with increasing favorable pressure gradient magnitude until eventually the sign of the heat transfer modification reverses, at sufficiently high  $St_r$ . The pattern of heat transfer modification with pressure gradient is very similar for high-speed disturbances, despite the decreased magnitude of the modification.

The implication of these heat flux modification calculations is that natural periodic vortex shedding or flow unsteadiness in the vicinity of a turbine blade can exert a significant influence on the measurement of heat transfer, and the magnitude of the influence can vary along the chord of the blade, as a function of the changing pressure gradient.

**6.3 Implications for Turbulent Flows.** Although the analysis performed in this study focused on a simplified model of laminar flow, the observations about the effect of critical layer velocity perturbations on heat transfer also raise important questions beyond laminar flows. Reference [23] and, later, Ref. [24] applied periodic oscillations to turbulent wall-bounded flows and also observed critical layer behavior, just like that observed in laminar flows. Indeed, Ref. [25] showed how the velocity modes associated with critical layers in turbulence can be used to model the dominant, energy-containing large-scale structures in turbulent flows. Moreover, Ref. [26] used traveling wave perturbations in the form of blowing and suction at the wall of a turbulent channel flow to achieve sublamina drag reduction, via their organizing effect on the Reynolds stress. References [27,28] have used acoustic traveling waves to modify heat transfer in compressible channel flows. In all of these cases, the same critical layer phenomena reported here for laminar flows has been observed to affect turbulent flows, too. Therefore, understanding the behavior of critical layer forcing on heat transfer in laminar flows has implications for the measurement and control of turbulent flows as well.

## 7 Discussion

The heat transfer and skin friction modification results obtained here can be applied to the turbine specific conditions explored in Sec. 4. Consider the case of the leading edge of a turbine airfoil experiencing fluctuations of the order of 7% due to a vortex street traveling at an inverse wave speed of  $c^{-1} = 1.6$ . The leading edge of this airfoil would experience a decrease in skin friction of nearly 40% and an increase in heat transfer of approximately 40%, purely due to streaming. Similarly, consider another case of the front section of a turbine airfoil under a favorable pressure gradient corresponding to an acceleration parameter,  $a_p$ , of  $-0.05$ , experiencing flow fluctuations of amplitude 10% due to small locally separated flow regions from the previous blade row, traveling at an inverse wave speed of  $c^{-1} = 2.8$ . This location of the blade would experience an increase of 80% in skin friction and a decrease of 30% in heat transfer, or Nusselt number, purely due to streaming. Therefore, streaming independently modifies the skin friction as well as heat transfer from the surfaces significantly. Two important conclusions can be drawn from this: (1) skin friction cannot be used to estimate heat transfer in the regimes of large unsteady flows, using the classical Reynolds analogy; and (2) numerical approaches that are unable to resolve the small scales of streaming and nonlinear interactions of fluctuations will likely miss the significant impacts of streaming on both skin friction and heat transfer.

Engine cycles are typically designed using reduced-order modeling tools with conservative safety factors that mitigate the risk associated with the ambiguity in turbine heat transfer based on a maximum allowable turbine blade temperature. For the

thermodynamic assessment of a viable engine, this results in conservatively constraining the turbine inlet temperature or overpredicting the coolant flow requirements. Consider a modern 2-spool unmixed turbofan with a fan pressure ratio of 2, a compressor pressure ratio of 20, a burner exit temperature of 1800 K, a turbine metal temperature of 1100 K, a bypass ratio of 10, and a 5% compressor air bleed for cooling the turbine guide vane and the rotor. We can then develop upper and lower bounds on the impact of a 30% change in Nusselt number due to the effect of streaming by assuming iso-heatflux or isothermal boundary conditions on the airfoil surface, which would translate to a 200 K variation in turbine inlet temperature or a 30% change in cooling air, respectively. The implications of these design requirement changes on engine efficiency were estimated using commercial GASTURB 11 software. For the iso-heat flux condition, the difference in permissible gas temperature is equivalent to increasing the core pressure ratio from 20 to 45, yielding an increase of about 4% in core efficiency. For the isothermal wall condition, the reduction in coolant flow consumption benefits the core efficiency by up to 0.3%. In reality, the turbine blade's boundary conditions lie somewhere between these two theoretical limits. In any case, considering streaming effects in the preliminary design stage can reduce the ambiguity in turbine heat transfer, thereby narrowing unnecessarily conservative safety margins and potentially yielding higher efficiency and predictive reliability for future engines.

Discrepancies between steady and unsteady uncooled turbine heat transfer measurements have plagued a wide range of experimental measurements. Specifically, a large difference in heat transfer measurements has been reported between uncooled vanes in linear cascade studies and those measured in rotating facilities [2,29,30]. This divergence in the experimental data has typically been attributed to the unsteady nature of the flow in the wake of the rotor, which was claimed to alter the turbine blade heat transfer coefficient by up to 50% [3], although no mechanism was identified. However, the present effort provides a mechanistic explanation for this phenomenon by means of perturbation-induced streaming. Using numerical solutions of a model flow over a turbine blade, the streaming effect was calculated to exert a modest impact on the skin friction factor, and a significant modification to surface heat transfer, far beyond values predicted by the Reynolds analogy. This streaming-based heat transfer enhancement was most prominent for downstream traveling wakes with significant velocity deficits compared to the freestream velocity, rather than upstream or downstream traveling acoustic excitations.

Since the streaming phenomenon can occur naturally due to the presence of unsteady flow features, it can lead to unaccounted heat flux enhancement when compared to undisturbed flow. Therefore, the thermal impact of streaming should be taken into consideration during the early design stages and when planning experimental measurements of heat transfer in rotating rig configurations. Moreover, it is clear that cascade testing, which typically does not include any representation of unsteadiness, cannot capture the impact of streaming on heat transfer.

The streaming effect also poses challenges for computational simulations of turbine flow. Since the streaming occurs in the Stokes layer extremely close to the wall, unsteady Reynolds-averaged Navier–Stokes (URANS) solvers, which typically implement wall functions for  $y^+ \sim 1 - 10$  to resolve the flow properties in the near-wall region [31], are inherently unable to capture this phenomenon. If LES models are used instead, the selected spatial and temporal discretization must be small enough to enable observation of streaming layers, leading to relatively high computational costs.

Validation of the current numerical approach in both the momentum and heat transfer domains has been performed against various experimental and exact numerical calculations under various perturbation conditions. The simplest case of the momentum transport in a laminar boundary layer subjected to temporal oscillations had previously been validated [9] against the experiments performed by Ref. [32] regarding the wall-normal profiles of the magnitude and

phase of streamwise velocity modes. For the case of a traveling wave perturbation, our momentum calculations also showed good agreement [9] with the experiments of Ref. [33], for the case of downstream traveling waves ( $c^{-1} = 1.67$ ). Extending the validation to include both momentum and heat transfer enhancement, we compared the predicted skin friction and heat transfer modifications for purely temporal oscillations to the boundary layer experiments of Ref. [34] at approximately matched Reynolds numbers of  $4 \times 10^5$ . Both our calculations and the experiments consistently showed no change in skin friction and heat transfer for the temporal oscillation ( $c^{-1} = 0$ ) case, as expected in the absence of critical layer effects [9]. To validate the case of traveling wave perturbations for both momentum and heat transfer, we compared our results to the linearized Navier–Stokes simulations performed by Ref. [35] in a laminar channel flow. In these studies at  $Re_{\delta^*} = 500$ , an optimum heat transfer modification and skin friction modification was observed at a phase speed expressed in terms of the bulk velocity  $U_p = c/U_b = 0.75$ , equivalent to  $c^{-1} = 2.7$ . For traveling waves of 15% amplitude ( $\epsilon = 0.15$ ), Ref. [35] reported skin friction modifications ( $\Delta C_f/C_f$ ) of 380% and heat transfer modifications ( $\Delta h_f/h_f$ ) of 880%, which compares well to our boundary layer results (despite the different geometries), which predict  $\Delta C_f/C_f$  of 180% and  $\Delta h_f/h_f$  of 1100% for a similar range of parameters,  $(c^{-1}, \epsilon, Re_*, Re_1) = (2.8, 0.15, 5 \times 10^3, 2 \times 10^4)$ . Of course, it is essential to recognize the difference between fully developed channel flow and a developing boundary layer. In the channel, Ref. [35] observed an optimum heat and momentum transfer enhancement at a fixed phase speed. In contrast, in our boundary layer study, the optimal phase speed varies with downstream distance as the boundary layer develops. But despite this difference, comparisons between the two geometries indicated strong qualitative and quantitative agreement.

## 8 Conclusion

The present analysis provides a tool to directly forecast the impact of zero-mean fluctuations on the turbine airfoil thermal performance. Due to streaming, the thermal performance of a system is significantly impacted by unsteadiness, especially for fluctuations that travel with low convective velocities (such as wakes). This impact is quadratically proportional to the amplitude of the fluctuations, making it particularly relevant for systems such as turbines that experience large amplitude unsteadiness. The study also found that the Reynolds analogy is not applicable in such conditions, and skin friction data should not be used to predict unsteady heat transfer behavior. The simple numerical model and results presented here offer a new perspective on how to reconcile the mismatch in the unsteady experimental data previously reported for uncooled turbine geometries, and a cautionary note for future experiments and simulations of unsteady heat transfer in turbomachinery. However, it should be noted that this tool presents a simplified analysis by neglecting spanwise effects to focus on the scaling trends in flow physics. Therefore, caution should be exercised in extending the recommendations of this tool to flows dominated by 3D effects, which might contribute to flow instabilities and spanwise coherent structures like streaks [15], especially at higher Reynolds numbers.

## Funding Data

- The Israel Science Foundation (Grant No. 1704/17).
- The US-Israel Binational Science Foundation (Grant No. 2016358).
- The Minerva Foundation (Grant No. AZ5746940764).

## Conflict of Interest

There are no conflicts of interest.

## Data Availability Statement

The datasets generated and supporting the findings of this article are obtainable from the corresponding author upon reasonable request.

## Nomenclature

$f$	= nonlinear forcing
$\ell$	= length scale
$p$	= static pressure
$t$	= time
$u$	= streamwise velocity
$v$	= wall-normal velocity
$x$	= streamwise coordinate
$y$	= wall normal coordinate
$\tilde{k}$	= wave number ( $m^{-1}$ )
$U$	= steady velocity at the freestream
$T$	= stretched time
$X$	= stretched streamwise coordinate
$Y$	= stretched wall normal coordinate
$\hat{C}$	= airfoil chord (m)

## Greek Symbols

$\hat{\alpha}$	= thermal diffusivity ( $m^2 s^{-1}$ )
$\Theta$	= temperature
$\hat{\nu}$	= kinematic viscosity ( $m^2 s^{-1}$ )
$\rho$	= fluid density
$\hat{\omega}$	= angular frequency of oscillations ( $rad s^{-1}$ )

## Dimensionless Numbers

$c$	= wave speed, $\hat{\omega}/\hat{k}$
$a_p$	= freestream acceleration parameter
$h_f$	= coefficient of heat transfer
$C_f$	= skin friction coefficient
$C_p$	= coefficient of static pressure
Pr	= Prandtl number, $\hat{\nu}/\hat{\alpha}$
$Re_1$	= streaming Reynolds number, $\hat{U}^2/\hat{\nu}\hat{\omega}$
$St_x$	= Strouhal number based on streamwise distance, $\hat{\omega}\hat{x}/\hat{U}$
$y^+$	= length scale for wall normal distance in CFD
$\epsilon$	= amplitude of fluctuations, $\hat{u}_1/\hat{U}$

## Superscripts and Subscripts

$q$	= nondimensional quantities
$\hat{q}$	= dimensional quantities
$\bar{q}$	= time averaged
$q'$	= fluctuating
$q_1$	= imposed fluctuations
$q_{\Theta}$	= thermal
$q_{\infty}$	= freestream quantity
$q_0$	= unforced case

## References

- [1] Dunn, M. G., 2001, "Convective Heat Transfer and Aerodynamics in Axial Flow Turbines," *ASME. J. Turbomach.*, **123**(4), pp. 637–686.
- [2] Han, J.-C., Zhang, L., and Ou, S., 1993, "Influence of Unsteady Wake on Heat Transfer Coefficient From a Gas Turbine Blade," *ASME. J. Heat. Transfer-Trans. ASME*, **115**(4), pp. 904–911.
- [3] Wright, L., and Schobeiri, M. T., 1999, "The Effect of Periodic Unsteady Flow on Aerodynamics and Heat Transfer on a Curved Surface," *ASME. J. Heat. Transfer-Trans. ASME*, **121**(1), pp. 22–33.
- [4] Schobeiri, M. T., Öztürk, B., Kegalj, M., and Bensing, D., 2008, "On the Physics of Heat Transfer and Aerodynamic Behavior of Separated Flow Along a Highly Loaded Low Pressure Turbine Blade Under Periodic Unsteady Wake Flow and Varying of Turbulence Intensity," *ASME. J. Heat. Transfer-Trans. ASME*, **130**(5), p. 051703.
- [5] Sigurdson, L. W., and Roshko, A., 1988, "The Structure and Control of a Turbulent Reattaching Flow," *Turbulence Manage. Relaminarisation*, **298**, pp. 497–514.

- [6] Cukurel, B., Selcan, C., and Stratmann, M., 2015, "Convective Heat Transfer Investigation of Acoustically Excited Flow Over an Isolated Rib Obstacle," *Int. J. Heat. Mass. Transfer.*, **91**, pp. 848–860.
- [7] Agarwal, T., Stratmann, M., Julius, S., and Cukurel, B., 2021, "Exploring Applicability of Acoustic Heat Transfer Enhancement Across Various Perturbation Elements," *ASME J. Turbomach.*, **143**(3), p. 031001.
- [8] Schubauer, G. B., and Skramstad, H. K., 1947, "Laminar Boundary-Layer Oscillations and Stability of Laminar Flow," *ASME. J. Aeronaut. Sci.*, **14**(2), pp. 69–78.
- [9] Agarwal, T., Cukurel, B., and Jacobi, I., 2022, "Localized Drag Modification in a Laminar Boundary Layer Subject to Free-Stream Travelling Waves via Critical and Stokes Layer Interactions," *J. Fluid. Mech.*, **937**, p. A10.
- [10] Lin, C., 1957, "Motion in the Boundary Layer With a Rapidly Oscillating External Flow," 9th International Congress of Applied Mechanics, Brussels, Belgium, Sept. 5–13.
- [11] von Karman, T., and Millikan, C., 1934, On the Theory of Laminar Boundary Layers Involving Separation, NASA Technical Report No NACA-TR-504, USA.
- [12] Howarth, L., and Bairstow, L., 1938, "On the Solution of the Laminar Boundary Layer Equations," *Proc. R. Soc. Lond. Ser. A - Math. Phys. Sci.*, **164**(919), pp. 547–579.
- [13] Telionis, D. P., 1981, *Unsteady Viscous Flow*, Springer-Verlag, New York.
- [14] Sommer, T. P., So, R. M. C., and Zhang, H. S., 1994, "Heat Transfer Modeling and the Assumption of Zero Wall Temperature Fluctuations," *ASME. J. Heat. Transfer-Trans. ASME.*, **116**(4), pp. 855–863.
- [15] Tiselj, I., Pogrebnyak, E., Li, C., Mosyak, A., and Hetsroni, G., 2001, "Effect of Wall Boundary Condition on Scalar Transfer in a Fully Developed Turbulent Flume," *Phys. Fluids.*, **13**(4), pp. 1028–1039.
- [16] 2015, *The Jet Engine*, Wiley, Manhattan, NY.
- [17] Acharya, S., and Mahmood, G., 2006, "Turbine Blade Aerodynamics," *The Gas Turbine Handbook*, Vol. 1, NETL, USA, pp. 364–380.
- [18] Green, R. B., Galbraith, R. A. M., and Niven, A., 1992, "Measurements of the Dynamic Stall Vortex Convection Speed," *Aeronaut. J.* (1968), **96**(958), pp. 319–325.
- [19] Lin, C., and Hsieh, S.-C., 2003, "Convection Velocity of Vortex Structures in the Near Wake of a Circular Cylinder," *J. Eng. Mech.*, **129**(10), pp. 1108–1118.
- [20] Del Álamo, J. C., and Jimenez, J., 2009, "Estimation of Turbulent Convection Velocities and Corrections to Taylor's Approximation," *J. Fluid. Mech.*, **640**, pp. 5–26.
- [21] Sieverding, C. H., Ottolia, D., Bagnera, C., Comodoro, A., Brouckaert, J. -F., and Desse, J.-M., 2004, "Unsteady Turbine Blade Wake Characteristics," *ASME J. Turbomach.*, **126**(4), pp. 551–559.
- [22] Porreca, L., Hollenstein, M., Kalfas, A. I., and Abhari, R. S., 2007, "Turbulence Measurements and Analysis in a Multistage Axial Turbine," *J. Propul. Power.*, **23**(1), pp. 227–234.
- [23] Hussain, A. K. M. F., and Reynolds, W. C., 1970, "The Mechanics of an Organized Wave in Turbulent Shear Flow," *J. Fluid. Mech.*, **41**(2), pp. 241–258.
- [24] Jacobi, I., and McKeon, B. J., 2011, "Dynamic Roughness Perturbation of a Turbulent Boundary Layer," *J. Fluid. Mech.*, **688**, pp. 258–296.
- [25] McKeon, B. J., and Sharma, A. S., 2010, "A Critical-Layer Framework for Turbulent Pipe Flow," *J. Fluid. Mech.*, **658**, pp. 336–382.
- [26] Min, T., Kang, S. M., Speyer, J. L., and Kim, J., 2006, "Sustained Sub-laminar Drag in a Fully Developed Channel Flow," *J. Fluid. Mech.*, **558**, pp. 309–318.
- [27] Rahbari, I., and Paniagua, G., 2020, "Acoustic Streaming in Turbulent Compressible Channel Flow for Heat Transfer Enhancement," *J. Fluid. Mech.*, **889**, p. A2.
- [28] Rahbari, I., Cukurel, B., and Paniagua, G., 2021, "Acoustic Pulsation for Heat Transfer Abatement in Supersonic Channel Flow," *Phys. Fluids.*, **33**(3), p. 035104.
- [29] Dring, R. P., Blair, M., Joslyn, H. D., Power, G., and Verdon, J., 1987, "The Effects of Inlet Turbulence and Rotor/Stator Interactions on the Aerodynamics and Heat Transfer of a Large-Scale Rotating Turbine Model—Volume 1," Technical Report No. E-3536, NASA.
- [30] Dullenkopf, K., Schulz, A., and Wittig, S., 1991, "The Effect of Incident Wake Conditions on the Mean Heat Transfer of an Airfoil," *ASME J. Turbomach.*, **113**(3), pp. 412–418.
- [31] Fluent ANSYS, 2011, "ANSYS Fluent Theory Guide," ANSYS Inc., Canonsburg, PA, pp. 724–746.
- [32] Hill, P. G., and Stenning, A. H., 1960, "Laminar Boundary Layers in Oscillatory Flow," *J. Basic. Eng.*, **82**(3), pp. 593–607.
- [33] Patel, M. H., 1975, "On Laminar Boundary Layers in Oscillatory Flow," *Proc. R. Soc. A: Math., Phys. Eng. Sci.*, **347**(1648), pp. 99–123.
- [34] Biles, D., 2019, "Experimental Investigations of Thermal Pulsatile Boundary Layer Flow," Ph.D. Dissertation, University of New Hampshire, Durham, NH.
- [35] Kaithakkal, A. J., Kametani, Y., and Hasegawa, Y., 2021, "Dissimilar Heat Transfer Enhancement in a Fully Developed Laminar Channel Flow Subjected to a Traveling Wave-Like Wall Blowing and Suction," *Int. J. Heat. Mass. Transfer.*, **164**, pp. 120485.